


RESEARCH ARTICLE

WILEY

Seismic response of floating wind turbines due to seaquakes

Amir M. Kaynia^{1,2}  | Håvard Blekastad³ | Philip Schell⁴ | Erik Løkken Walter⁵¹Norwegian University of Science and Technology (NTNU), Trondheim, Norway²Norconsult AS, Sandvika, Norway³Norconsult AS, Kristiansand, Norway⁴Dr.ing. Aas-Jakobsen AS, Oslo, Norway⁵Dr.techn. Olav Olsen AS, Lysaker, Norway**Correspondence**

Amir M. Kaynia, Norwegian University of Science and Technology (NTNU), Trondheim, Norway.

Email: amir.kaynia@ntnu.no**Funding information**

There was no research funding for this study.

Abstract

Vertical seismic waves, which are primarily due to pressure waves in the ground, can propagate with the same intensity in the seawater and impact floating bodies such as floating wind turbines (FWTs). Part of this wave can further propagate in the tower and generate large vertical accelerations in the nacelle. This paper presents a methodology for computation of the pressure waves generated by vertical earthquake shaking, referred to as seaquake, its impact on submerged bodies, and the induced dynamic response in the structure. A FWT concept with catenary mooring is used for the assessment of the effects of earthquake shaking. The pressure during a seaquake is determined using a 2D acoustic finite element (FE) model in Abaqus. The acoustic model is benchmarked against a 1D analytical solution. The response due to the environmental loads, namely, wind, current, and waves, is also studied and used as a reference for assessment of the relative significance of the seaquake. Considerable vertical accelerations can occur in the nacelle due to amplification of the platform accelerations through the tower. It is shown that this acceleration could exceed a commonly used operational limit range of 0.2 g to 0.3 g even for moderate accelerations at the seabed. This indicates that earthquake loading should be considered in the design of FWTs in seismic regions. The mooring tensile forces, due to motion of the platform during a seaquake, do not exceed the design tension computed for the extreme environmental conditions. However, the leeward mooring lines could experience zero tension, which could cause snap tension.

KEYWORDS

finite element, floating wind turbine, mooring, seaquake, seismic loading, SIMA model, structural dynamics, wind tower

1 | INTRODUCTION

Wind energy will represent an important part of the production of renewable energy in the years to come. Europe, United States, and many East Asian countries are all leaning towards solutions based on renewable energy. For example, the European Union decided already in 2009 that 20% of the energy consumption of the continent should be provided by renewable sources by the year 2020.¹ Several European countries, including Denmark and UK, have set very ambitious plans for replacing fossil energy with renewable energy in the near future. Wind energy is a strong contributor to renewable energy; however, considering the various environmental and space challenges with onshore wind energy installations, more

This is an open access article under the terms of the [Creative Commons Attribution-NonCommercial-NoDerivs](https://creativecommons.org/licenses/by-nc-nd/4.0/) License, which permits use and distribution in any medium, provided the original work is properly cited, the use is non-commercial and no modifications or adaptations are made.

© 2022 The Authors. *Wind Energy* published by John Wiley & Sons Ltd.

focus is being given to offshore wind energy. Offshore wind has become an attractive alternative also thanks to more stable energy due to wind conditions offshore.

Most offshore wind farms are developed with fixed-bottom foundations such as monopiles, steel jackets on piles or suction caissons. The main limiting factor for fixed-bottom offshore structures is the water depth. Wind turbines with fixed foundations are limited to depths up to 50–60 m due to design, construction, and cost challenges.¹ Therefore, floating wind turbines (FWTs) are being more deployed in regions with larger water depths. For many countries, fixed-bottom offshore wind parks are not an option due to the topography of the seabed or sudden and steep drops of the continental shelf, such as in northern Europe. Projects with FWTs have already been developed in Norway. One example is Equinor's Hywind Demonstrator project which involved installation of a FWT outside of Karmøy in Norway in 2009.² Currently, many wind farms are under development across the world.

There is a considerable experience in the oil and gas industry with floating offshore construction and mooring systems that are being considered for FWTs. The three main configurations are semi-submersible, spar, and tension leg platform (TLP) as schematically illustrated in Figure 1. A semi-submersible platform is partially submerged and consists of underwater pontoons supporting the outer columns. The platform is usually anchored to the seabed with catenary or semi-taut mooring lines (MLs). The stability is achieved primarily by the large water plane area. A Spar comprises a hollow cylindrical hull, and its stability is achieved by having a center of gravity in the water deeper than the center of buoyancy. In practice, this is done using ballast in the lower part. The platform is kept in place most commonly by a catenary mooring system. Finally, TLP is the type of floating structure that is anchored to the seabed by vertical tendons in tension. The tension should always be large enough to avoid slack in the tendons. An additional challenge in TLPs is the design of anchors which are always under a static uplift and cyclic loads due to vertical oscillations of the platform. In this study, a recent FWT concept of the family of semi-submersibles is used for the analyses. However, the adopted models and tools are equally applicable or readily extendable to other types of FWTs.

The seismic compressional waves in the ground, which produce vertical motion on the seabed during an earthquake, create pressure waves in the seawater that propagate towards the water surface. This has been referred to as a *sequake* (e.g., Hove et al.³). The impact of sequake waves on floating structures and ships can damage these structures. There are numerous examples where ships have experienced the pressure waves produced by an earthquake. One destructive incident was on the Norwegian ship called "MT Ida Knudsen". In 1969, the ship suffered critical damage during an earthquake off the west coast of Gibraltar. The sequake resulted in damages in the hull and disabled some of the machinery on board.⁴ Another example is the Kobe earthquake in 1995. It was reported that four ships in the Osaka Bay experienced two shock waves during the earthquake.⁵ The pressure waves from seaquakes could present a real threat to FWTs and other floating structures; moreover, the induced acceleration from the pressure waves could damage the various components in the turbines, especially the nacelle.

The research on the effect of seaquakes on floating structures has been mostly based on decoupled methods through the following two steps: (i) the pressure from the seismic pressure waves on the submerged structure is computed either by analytical solutions with idealized geometries or through boundary element (BE) and finite element (FE) solutions assuming the structure is rigid (i.e. reflecting boundary) and (ii) the response of the structure to the contact pressures determined in the first step is computed by different models. A host of solutions have been presented for the solution of wave propagation described in the first step (e.g., earlier studies^{6,7}). Several researchers (e.g., Higo and Ueno⁸) used the Green's functions for acoustic waves and applied it in a BE formulation to account for the boundary conditions and computed the pressures and associated sequake forces on 3D floating bodies. A different approach used the analytical solutions for pulsating bubbles and by

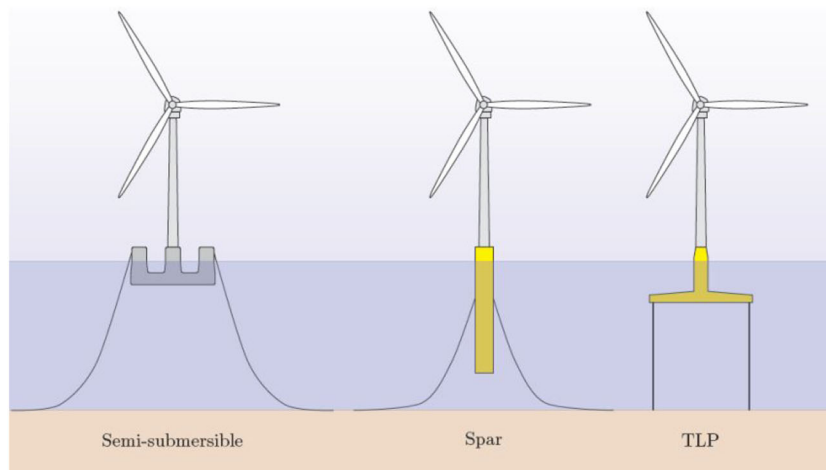


FIGURE 1 Common floater types for wind turbines

representing the seabed with distributed pulsating bubbles, computed the seaquake pressures on floating rigid bodies.⁹ This study also used an experimental set up with a shake table to generate lateral waves, representing water waves in a basin, and measured motions of a floating body. The study reported in Takamura et al.¹⁰ solved the Helmholtz equation for velocity potential in a two-dimensional space and computed the hydrodynamic pressure on a rigid floating structure. The study provided insight into the effect of frequency and impedance characteristics of the ground on the computed pressures. The BE method was used in Fujioka et al.¹¹ to solve the equation for the velocity potential in 2D and 3D dimensions. For 2D cases, the study computed the pressures on rigid spars and pontoons with different dimensions. The source was varied from a limited area at the seabed to the whole breadth of the modeled domain. For the 3D case, the study considered an axisymmetric geometry with the spar platform in the center. The reported results showed the possibility for creation of large loads on a spar due to its relatively high natural frequency and possibility of resonance with the high-frequency pressure waves.

An important recent application of seaquake load has been related to design of submerged floating tunnels. Several methods inspired by the available analysis tools have been applied by the researchers.^{12–14} In some of these studies, the loads from the seismic waves on the tunnel have been represented by the Morison's equation for loads on vibrating bodies.¹⁵ See Martinelli et al.¹⁴ for a review of these studies and the analysis approaches for submerged tunnels.

The objective of this study is assessment of earthquake shaking on FWTs. The subject has been studied for fixed-bottom OWTs by numerous researchers, and most of the design issues have already been identified (see Kaynia¹⁶ for a review of some of the key issues in this subject). However, FWTs have received much less attention, because they are not influenced by the horizontal earthquake shaking, which is often the main source of damage to structures, as water cannot transmit shear waves. Compressional waves in the ground, on the other hand, can propagate in the seawater uninterruptedly and strike floating structures. Therefore, this study focuses on the effect of vertical ground shaking on the response of floating platforms and towers. Considering the large difference between the natural periods of FWTs with catenary or semi-taut mooring and the period of seismic pressure waves in water, a decoupled computational approach comprising a hydrodynamic load computation and a hydro-aero-elasto-dynamic model for the load effect on the structure is used. These steps and an example of application are discussed in the following sections.

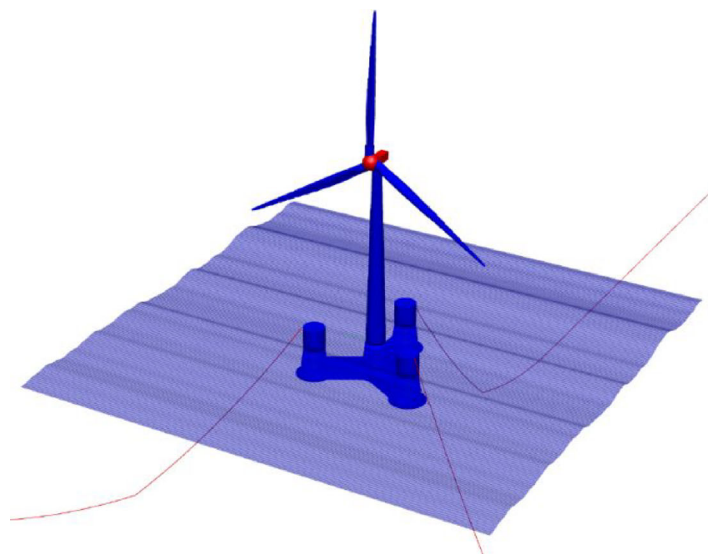
2 | PROBLEM STATEMENT AND SOLUTION STRATEGY

As explained above, FWTs are not vulnerable to horizontal earthquake shaking because the horizontal ground motions cannot be transferred by the seawater. Therefore, FWTs have a clear advantage over the fixed-bottom offshore wind turbines. Probably, the main earthquake challenge to FWTs is liquefaction of the soil which holds the anchors^{17,18}; however, it should be noted that liquefaction is even a larger threat to the performance of fixed-bottom OWTs as demonstrated in Esfeh and Kaynia.¹⁹ On the other hand, the seismic pressure waves in the ground could easily propagate in the seawater and affect the FWT. In addition to the inflicted pressure on the hull, the impact could induce a vertical wave in the tower resulting in a potentially large acceleration in the RNA and axial stresses in the tower. The acceleration tends to be large due to the low damping in the structure. The study reported in Kjølraug and Kaynia²⁰ for a fixed-bottom OWT has clearly shown the potential damaging effect of vertical shaking. A common industrial practice for the design of FWT is to set an operational limit in the range 0.2 g to 0.3 g for the accelerations in the top of the turbine tower.²¹ This limit is related to the performance of the turbine components in the nacelle.

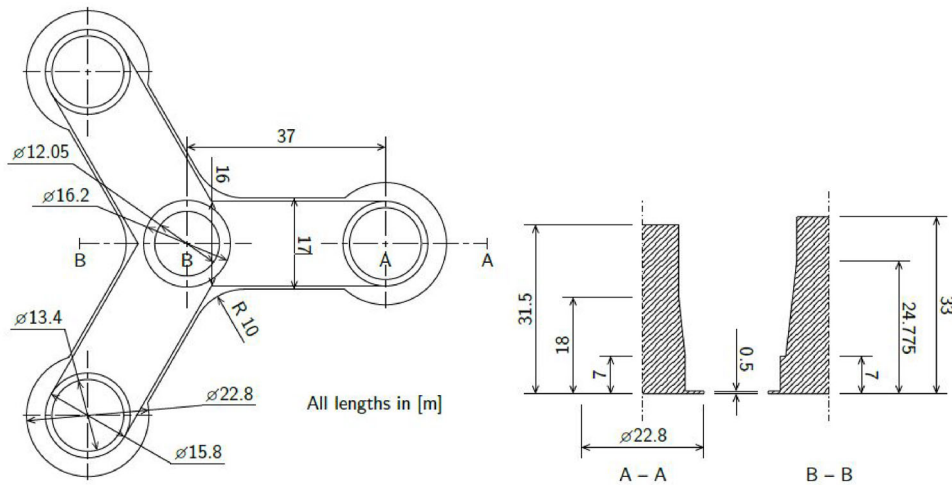
The analyses presented in this study were performed based on a decoupled approach. The first step is computation of the pressure field in the seawater due to the vertical oscillations of the seabed. For this purpose, the 2D and 3D acoustic models in the FE program Abaqus²² were used. The accuracy of the model was established through comparisons with a 1D analytical solution for harmonic acoustic waves in water. Due to the large difference between the natural frequency of the pressure waves and the natural frequencies of the FWT, the base of the FWT in contact with water was assumed fixed (reflecting boundary) when computing the pressure time histories. This decoupling approach is believed to lead to slightly conservative results because of a minor interaction of the structure with the seawater.

The second step is computation of the dynamic response of the FWT due to the pressure load computed in the first step. The effect of the seaquake on the FWT was investigated here using the hydro-aero-elasto-dynamic simulation code SIMA²³ that implements RIFLEX and SIMO as solvers for determination of the response of the flexible parts and rigid bodies of the FWT, respectively.

Over the past 10 years, an FWT concept known as the OO-Star Wind Floater²⁴ (denoted as OOSF for brevity in this paper) has been developed by Dr.techn. Olav Olsen AS and is owned by Floating Wind Solutions AS. As part of a research project funded by the European Commission's H2020 program (see Berthelsen et al.²⁵ and <https://lifes50plus.eu>), a robust design for a 10 MW OOSF was made public for research purposes. This version of the OOSF is applied in the present study for the assessment of the earthquake response. Figure 2A shows the geometry of OOSF together with the MLs as modeled in aero-hydro-elasto-dynamic code SIMA. Figure 2B gives the key dimensions of the platform, and Table 1 lists the key parameters of OOSF. The presented methodology in this paper is general and can be applied to any FWT or other floating structures. Selection of a specific design with known details in the present study has only made the computed results useful for general evaluations. A catenary mooring was considered for anchoring of the platform.



(A) Model presented in SIMA



(B) Key geometry data

FIGURE 2 (A, B) LIFES50+OO-Star Wind Floater semi 10 MW²⁵

TABLE 1 Parameters of the LIFES50+version of OO-Star Wind Floater 10 MW (including ballast) made available in lifes50plus.eu

Property	Unit	Value
Total platform mass	kg	2.171×10^7
Center of mass below SWL	m	15.225
Tower base interface above SWL	m	11.0
Draft at equilibrium position including mooring	m	22.0
Displaced water volume	m ³	2.351×10^4
Center of buoyancy below SWL	m	14.236

Abbreviation: SWL, still water level.

3 | MODELING OF SEISMIC SEAQUAKES WAVES

3.1 | Verification of numerical simulation tool

The FE analysis program Abaqus was used for computation of the compressional stress at the base of the platform assuming it as a rigid boundary/reflector. For verifying the model, the performance of Abaqus for this application was benchmarked against the results of a 1D analytical acoustic model as described in the following.

The differential equation of motion for pressure waves propagation in a 1D water column over a rigid base is given by

$$\frac{\partial^2 u}{\partial t^2} = V_p^2 \frac{\partial^2 u}{\partial z^2} \quad (1)$$

in which $u(z, t)$ is the particle motion and $V_p = (K_w/\rho_w)^{0.5}$ where K_w , ρ_w , and V_p are the bulk modulus, mass density, and pressure wave velocity of water, respectively, and z is the vertical coordinate axis along the water column with $z = 0$ at the base and $z = H$ on top of the water column. For excitation at the base with a harmonic frequency, ω , the above equation can be transformed to a simple ordinary differential equation. Solution of this equation, and application of the boundary conditions $u(0) = u_0$ together with zero pressure on the free surface, leads to the analytical solution of this equation. The transfer function between the base motion and maximum pressure at a point $z = h$ in the water column can then be derived readily as

$$H(\omega) = \frac{P}{u_0} = K_w k (\tan(kH) \cdot \cos(kh) - \sin(kh)) \quad (2)$$

where P is the amplitude of the pressure and $k = \omega/V_p$ is the wave number. Consistent with the applied boundary conditions, one gets zero pressure for $h = H$.

For cases with material damping, the bulk modulus can be replaced by its complex counterpart, $K_w^* = K_w (1 + 2\xi)$ where ξ is the damping ratio. For small damping ratios (e.g., less than 5%) Equation 2 can be approximately expressed as

$$H(\omega) \approx K_w k (1 + i\xi) \cdot (\tan(k(1 - i\xi)H) \cdot \cos(k(1 - i\xi)h) - \sin(k(1 - i\xi)h)) \quad (3)$$

For the analyses carried out in this study, the acceleration time history for the Loma Prieta earthquake recorded at Point Bonita, California, on October 18, 1989 (Figure 3), with a peak vertical acceleration PVA = 0.34 m/s² (~ 0.035 g), was used for the shaking at the base. While the analyses performed in this study and the conclusions reached are generally independent of the selected earthquake record, this time history was selected because it has relatively uniform energy in the frequency range 0.5 to 8 Hz which is typical for earthquake excitations.

For a given motion at the base, the acceleration time history can be transformed to the frequency domain by the Fourier transform (FT), the response can be computed in the frequency domain using the transfer function in Equation 3, and finally, the time history of the pressure at any point in the model can be computed by applying an inverse Fourier transform (IFT) of the pressure in the frequency domain.

This solution was applied in a 1D model with length 100 m. Figure 4A displays the computed time history of the pressure at a depth 22 m from the surface due to the vertical earthquake shaking with PVA = 0.035 g shown in Figure 3. This depth corresponds to the underside of the OOSF hull. Figure 4B displays the 3D simulation results by Abaqus in a model with side dimensions 5 m and length 100 m. The Abaqus model

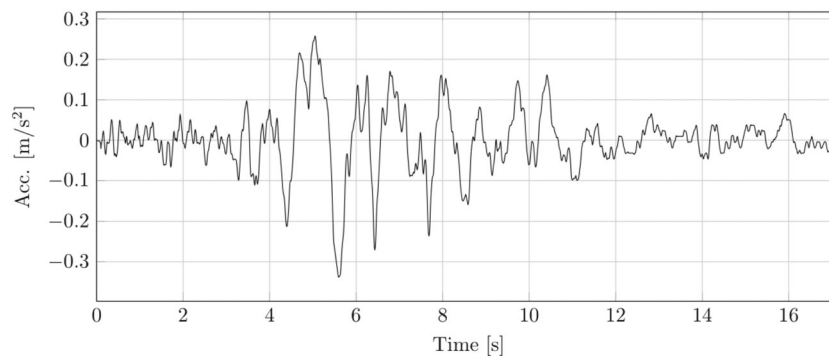


FIGURE 3 Acceleration time history of Loma Prieta, 1989, recorded at Point Bonita, California in vertical direction

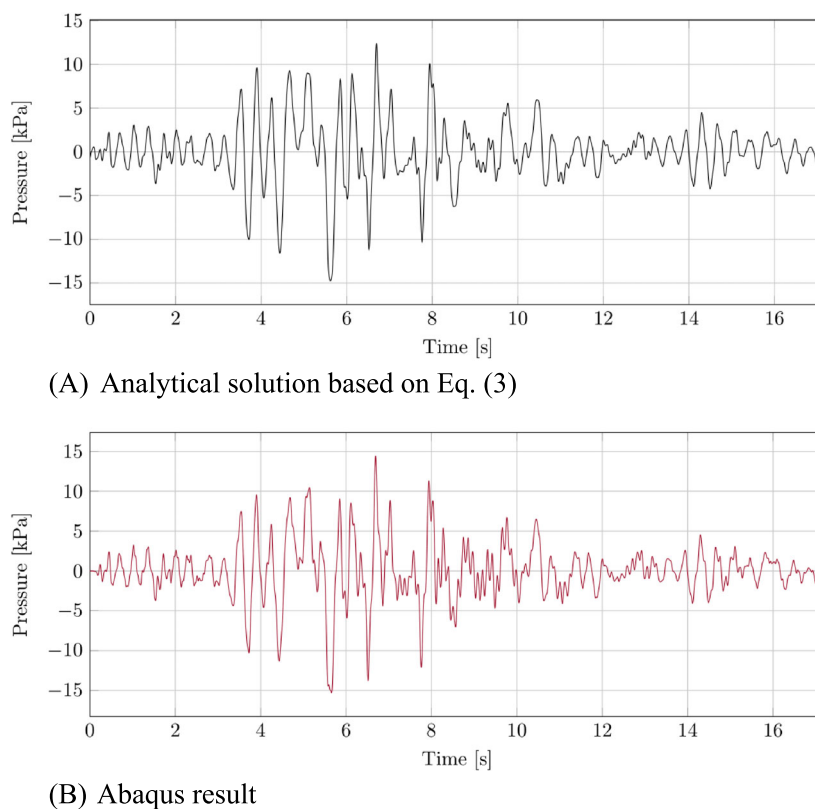


FIGURE 4 (A, B) Analytical and numerical (Abaqus) results for water pressure at 22 m from free surface

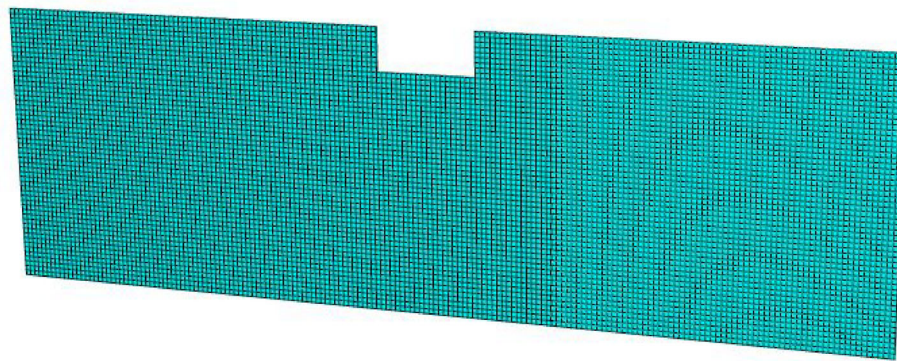
consisted of acoustic 3D elements of type AC3D8R with dimensions 1 m. The element size is significantly smaller than the maximum required element size which is about one tenth of the wavelength for the frequencies of interest. For vertical earthquake shaking with typical frequency content of up to 30 Hz, the shortest wavelength is about 50 m. A very good agreement is obtained between the two results which confirms satisfactory performance of the Abaqus acoustic model.

In real designs, one needs large FE models which computationally could become very demanding specially for FWTs in deep water. To address this challenge, the applicability of a 2D plane strain model (with a transverse dimension of 1 m) is evaluated in the next section. It is shown that such a model with sufficient lateral extent could provide an indication of the expected hydrodynamic pressures.

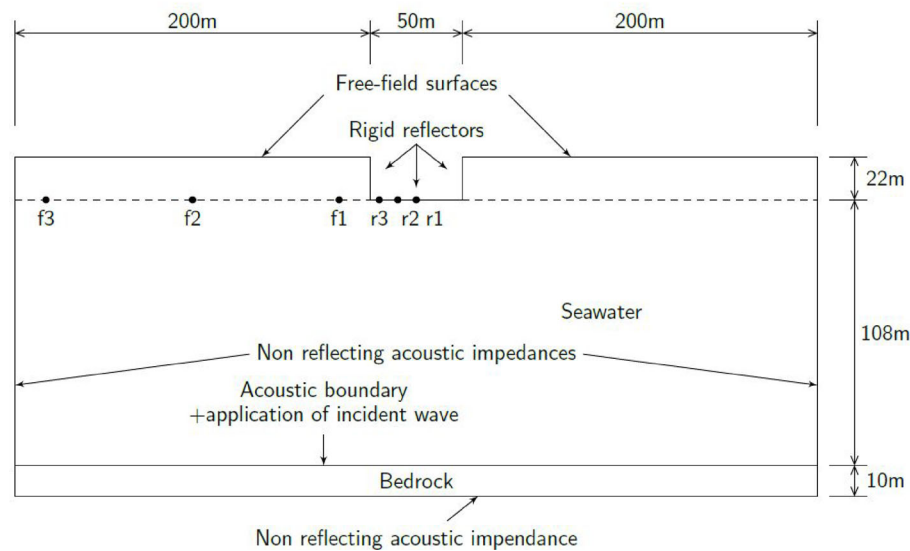
3.2 | Two-dimensional hydrodynamic simulations

Figure 5 illustrates the 2D acoustic FE model with water depth 130 m and lateral extent 450 m used for computation of the water pressures at the base of the platform. The base area of OOSF is approximately 2500 m². Therefore, the width of the rigid reflector, which represents the floater, was chosen to be 50 m. Nonreflective acoustic impedances were assigned to the bedrock and to the vertical side boundaries of the model. These impedances account for the loss of pressures horizontally which will occur when a large domain is considered. When compressional waves hit the platform, some of them will be reflected and refracted by the platform reflectors but will be absorbed by the lateral boundaries. The seabed (top of bedrock) was assumed horizontal, and it was assumed that all points along this surface experience the same vertical motion which is logical for points in a small region relative to the wavelength. This was achieved in the 2D acoustic model by using a planar incident wave to represent the vertical earthquake shaking. The same acoustic material properties, element type, time step, and integration method were used as in the verification model. The seabed was assumed to consist of bedrock with the following acoustic properties: mass density = 2500 kg/m³ and wave speed = 5500 m/s. The corresponding parameters in the seawater were taken equal to 1024 kg/m³ and sound speed = 1500 m/s. As shown in Figure 5, the bedrock half space was represented in the Abaqus model by a 10 m layer of rock with nonreflecting boundary at its base.

Six points were selected at the level of the base of the platform (Figure 5B). Points r1, r2, and r3 are on the rigid reflector, and points f1, f2, and f3 are in the free field. The objective was to compare the pressures at these points to find out to what extent the presence of the platform changes the free-field pressures. Obviously, it is expected that the pressures at the points r1–r3 be larger than those at the points f1–f3; moreover, the pressure should decrease in these points with distance from the platform.



(A) FE mesh in 2D Abaqus



(B) FE dimensions and boundary conditions (note: x and y dimensions are not to scale)

FIGURE 5 (A, B) Acoustic finite element (FE) model and properties

Figure 6A plots the time histories of the computed pressures at points r1–r3. As expected, there is minor difference between them with the point at the center having the largest values. Figure 6B displays the time histories of the pressures at points f1–f3. The pressures at these points are about half of those at the r-points with the largest value closest to the platform. As the distance from the platform increases, the pressure tends to the 1D free-field condition (compare Figure 6B with Figure 4B). This is an interesting and practically useful result as it demonstrates that one could obtain an approximate indication of the level of pressures on the platform from a simple 1D analytical solutions which can be easily applied to deep water cases. The fact that the pressure time history at the farthest point, f3, is close to the free-field pressures is a confirmation that the selected lateral model size of the FE model is satisfactory.

Figure 7 displays contour plots of the pressure in the model at arbitrarily selected time instances 3, 6, and 9 s. These figures clearly demonstrate the pressure field created due to the presence of the platform.

4 | MODELING OF DYNAMIC RESPONSE OF FWT

A computational model of OOSF was created in SIMA as shown in Figure 2A. SIMA²³ is a graphical user interface which executes different dynamic response solvers like SIMO and RIFLEX. The response of the model is solved by a coupled SIMO-RIFLEX analysis in SIMA that uses nonlinear beam elements for the tower and blades and bar elements for the MLs. These allow for large deflections and include nonlinear geometric stiffness. Additionally, nonlinear drag loads are included in the hydrodynamic load models. A drag coefficient $C_d = 1.9$ was used for the drag force on the thin plates at the base of the columns. The platform, nacelle, and hub are modeled as rigid bodies, and their responses are computed

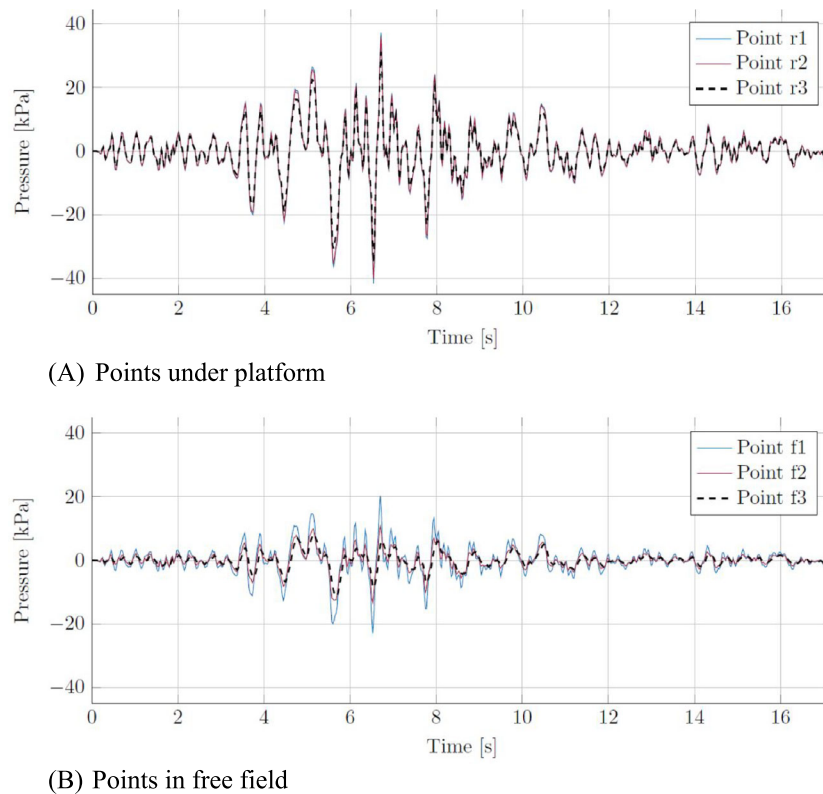


FIGURE 6 (A, B) Time histories of pressures computed from 2D Abaqus model

in SIMO. The model was initially developed as a contribution to the Horizon 2020 research project LIFES50+.²⁵ The model comprises a wind turbine based on the DTU 10-MW reference wind turbine,²⁶ mounted on the OOSF semisubmersible platform. The FWT is kept stationary by a catenary mooring system comprising chain anchor lines. The boundary condition of the catenary mooring system in the connection with the seabed is pinned with a normal stiffness of 15 kN/m.

Tables 2 and 3 list the parameters of the turbine tower and those of DTU 10 MW reference turbine.

A free-decay analysis was conducted to study the dynamic behavior of the FWT. Six separate analyses were performed, each by giving the turbine an initial displacement in the considered degree of freedom and allowing free vibration oscillations. Table 4 lists the measured natural periods and damping ratios from the free-decay oscillations. The values computed in LIFES50+ are also included for comparison. The damping ratios were calculated for different numbers of displacement peaks which show a diminishing trend with number of oscillations, because damping is dependent on velocity which reduces during the free-decay. The computed natural periods agree well with the values computed in LIFES50+ except in yaw where the values deviate by about 15%. This is believed to be due to slightly different mooring configuration as the only restoring forces involved in the yaw decay motion stem from the MLs.

With a secondary objective of exploring engineering tools for estimation of the response of FWT to vertical seismic shaking, an attempt was made to estimate the key dynamic characteristics in the heave direction by using a simple SDOF model. Figure 8 shows this model and the components of the SDOF system.

The stiffness and mass contribution from the mooring system in heave motion are small compared with the hydrostatic restoring forces for catenary moored floating structures.²⁷ Therefore, the stiffness of the system is only due to the hydrostatic restoring forces. By ignoring the weight of the MLs, the equilibrium heave position is where the hydrostatic restoring force is equal to the total weight of the FWT. If the cross-sectional area of the platform around this equilibrium position has a small enough variation, the hydrostatic stiffness in heave may be based on the cross-sectional area of the platform at still water level (SWL). The following are the parameters of the SDOF in Figure 8 extracted from the OOSF data in Figure 2B.²⁸

- Total mass of FWT, $M_{\text{tot}} = M_{\text{semi}} + M_{\text{rotor}} + M_{\text{nacelle}} + M_{\text{tower}} = 23,650$ tons
- Hydrodynamic added mass, $A_{33} = 35,800$ tons
- Hydrostatic stiffness in heave, $K_{33} = \rho_w g A_{\text{SWL}} = 5490$ kN/m.
- Cross-section area at SWL = $A_{\text{SWL}} = 547$ m²

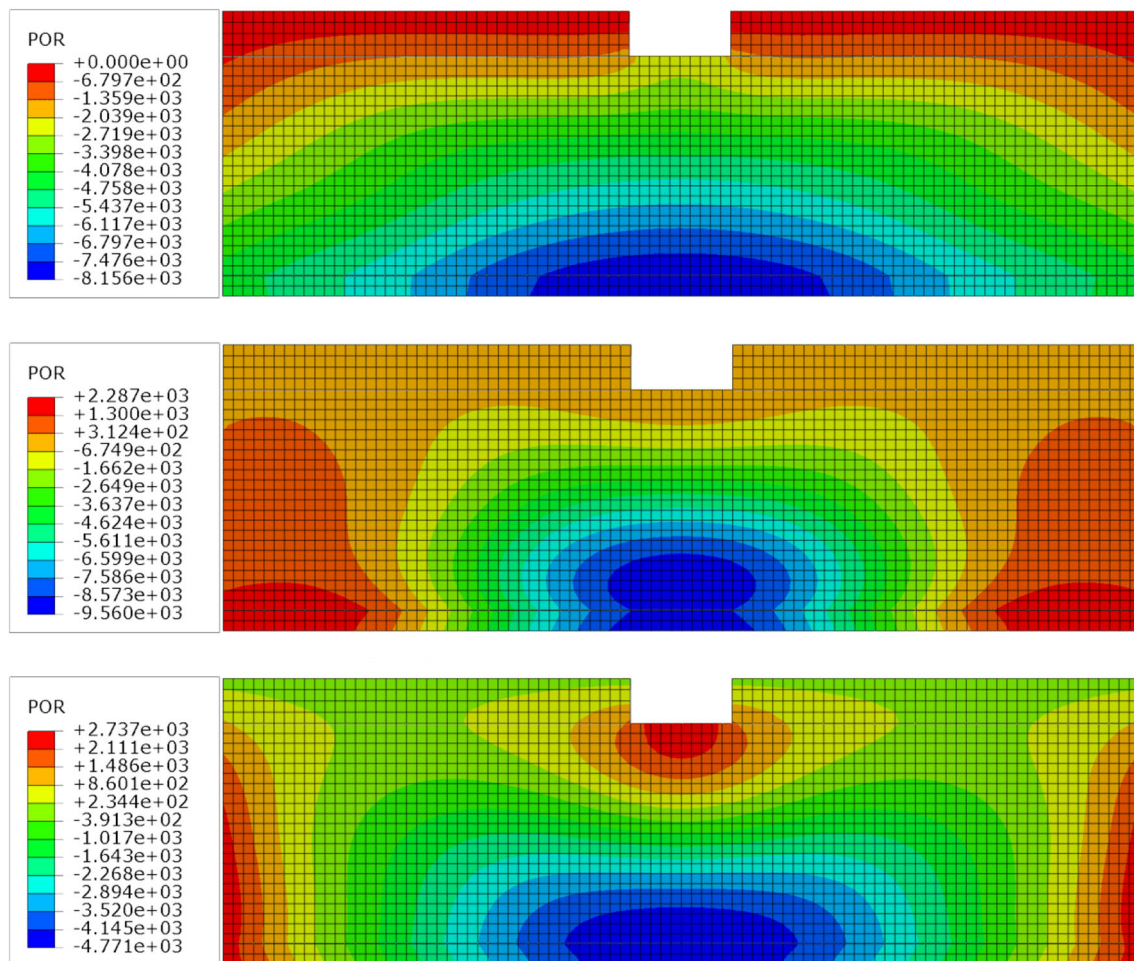


FIGURE 7 Contour plots for acoustic pressure after 3, 6, and 9 s. Pressures in the legend are in Pa.

TABLE 2 Parameters of wind turbine tower

Property	Unit	Value
Total mass	kg	1.257×10^6
Tower base elevation above SWL	m	11.0
Tower top elevation above SWL	m	115.63
Vertical center of mass above SWL	m	49.8
Density, ρ	kg/m ³	8.243×10^3
Modulus of elasticity, E	N/m ²	2.10×10^{11}

Abbreviation: SWL, still water level.

TABLE 3 Parameters of DTU 10 MW reference turbine

Property	Unit	Value
Rotor mass	kg	230,717
Rotor center of mass (x, y, z)	m	(-7.07, 0.0, 119.0)
Nacelle mass	kg	446,006
Nacelle center of mass (x, y, z)	m	(2.69, 0.0, 118.08)

TABLE 4 Free-decay motion characteristics from SIMA analyses

DOF	Damped natural period T_D (s)		Computed damping ratio ξ (%)			
	SIMA	LIFES50 + D4.2	Number of peaks after first			
			3	6	9	12
Surge	185.03	$1/0.0055 = 181.82$	2.796	2.337	2.021	1.800
Sway	184.97	-	2.781	2.316	2.004	1.783
Heave	20.83	$1/0.049 = 20.41$	0.419	0.406	0.395	0.385
Roll	31.84	-	2.193	1.339	1.512	1.144
Pitch	31.80	$1/0.032 = 31.25$	1.768	1.047	1.214	0.930
Yaw	99.29	$1/0.0086 = 116.28$	2.096	1.833	1.645	1.503

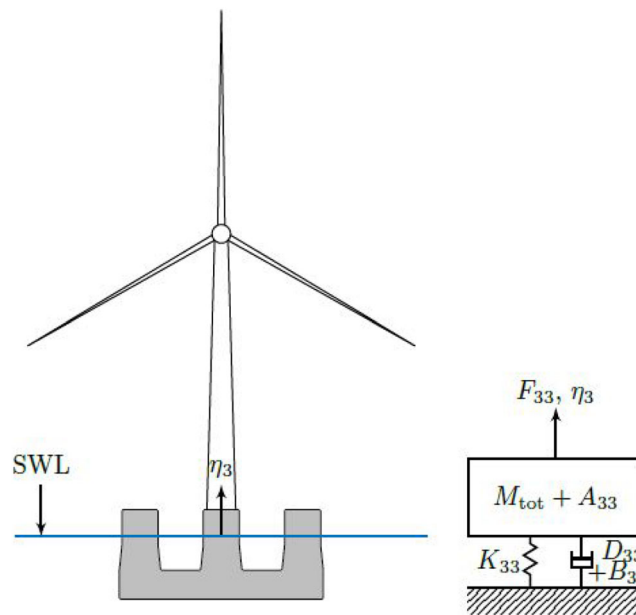
**FIGURE 8** Heave motion modeled as SDOF system

Figure 9 shows the results of computation of the added mass and damping as functions of frequency from SIMA. Using the above values, one gets the natural period for the SDOF system equal to 19.9 s which deviates by only 5% from the value obtained during the free-decay analysis and the value given in LIFES50+ report.

5 | NUMERICAL SIMULATIONS

To assess the importance of seaquake on dynamic response of FWTs, several analyses were performed in SIMA for wave and wind loading and separately by including seaquake loading. The parameters describing the wind, wave, and current acting on the wind turbine were gathered from the LIFES50+ report²⁹ describing oceanographic and meteorological conditions at three different sites suitable for offshore wind development. The selected parameters are also presented in the following sections.

5.1 | Earthquake response in calm environment

To assess the significance of earthquake shaking, a calm environment (that is, without wind and current loads) was considered first. At the time of applying the seaquake pressures in SIMA, the buoyant forces described by the hydrostatic stiffness matrix, the weight of the structure, and the forces acting on the platform from the MLs are not fully in equilibrium. This yields an initial movement of the wind turbine which slowly decays

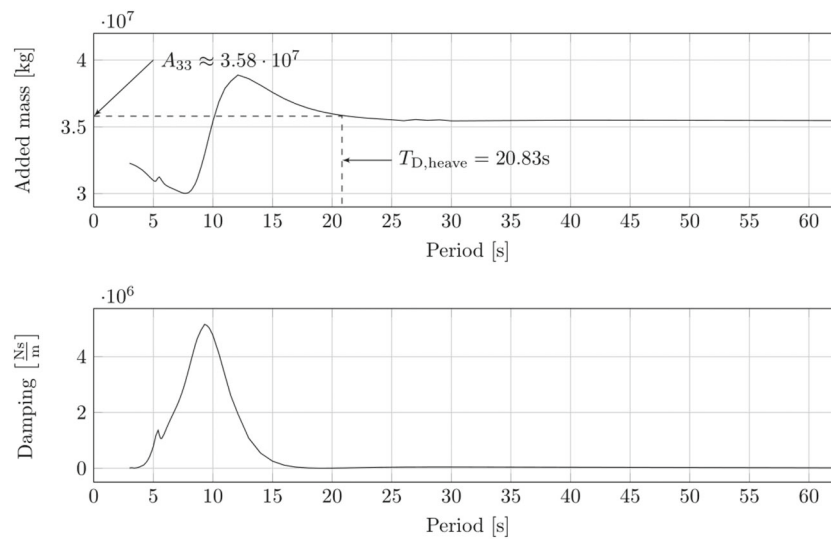


FIGURE 9 Frequency-dependent added mass and damping of platform in heave motion computed from SIMA model

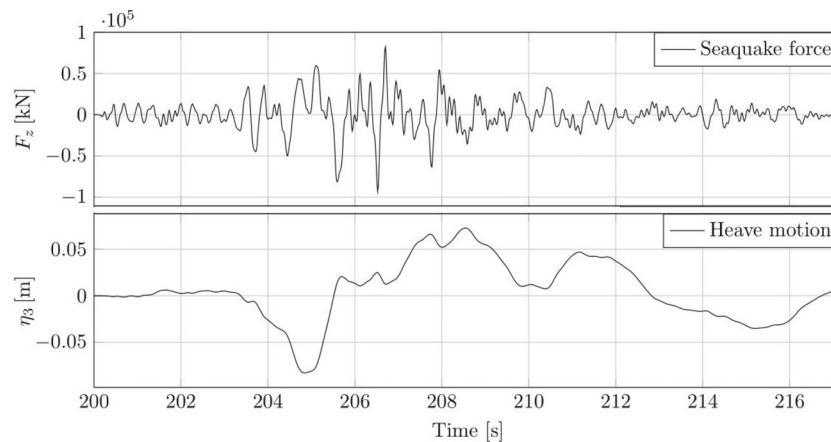


FIGURE 10 Response of floating wind turbine (FWT) subjected to the average seaquake pressure from 2D acoustic model

with time. To accelerate decay of the vibrations caused by the initial conditions, additional (fictitious) damping was introduced in the form of viscous dashpots before applying the seaquake loads at time 200 s.

Figure 6A plots the values of the computed seaquake pressures at different points on the base of the platform. These pressures were averaged along the bottom of the platform and applied as a single concentrated time-varying force as shown in Figure 10. The same figure (bottom plot) displays the time history of the computed heave of the platform which indicates a moderate heave motion of about 8.5 cm.

Figure 11 displays the response of the nacelle in terms of both displacement and acceleration. The vertical acceleration levels (peak value about 0.26 g) are in the operational limit range (see Section 6 for a discussion on the significance of the peak accelerations in assessing the response of the nacelle). The large amplification of ground accelerations is for two reasons. The first is due to the amplification of motions in the water because the natural frequency of the water column is about 3 Hz which is in the range where most of the earthquake energy is concentrated. This amplification is therefore independent of the type of FWT. This issue is further elaborated in Section 6. The second reason for amplification is that the vertical natural frequency of most towers is close to the range of dominant frequencies in vertical earthquake shaking. To elucidate this, the information about the first four modes of the vertical structural vibration of the tower are listed in Table 5. The tower model in SIMA was discretized into 27 circular tube segments with a constant diameter and wall thickness within each segment. Each of these was represented by one beam element. The table also includes the modal damping ratios. As the results indicate, the first mode has a dominant modal participation, and its frequency is clearly discernable in the acceleration time history in Figure 10. There is often very little energy in the earthquake shaking for the higher modes and their participation quickly vanishes. Therefore, even though the damping ratios in the modes computed by the Rayleigh damping are unrealistically high, they have no practical impact on the results.

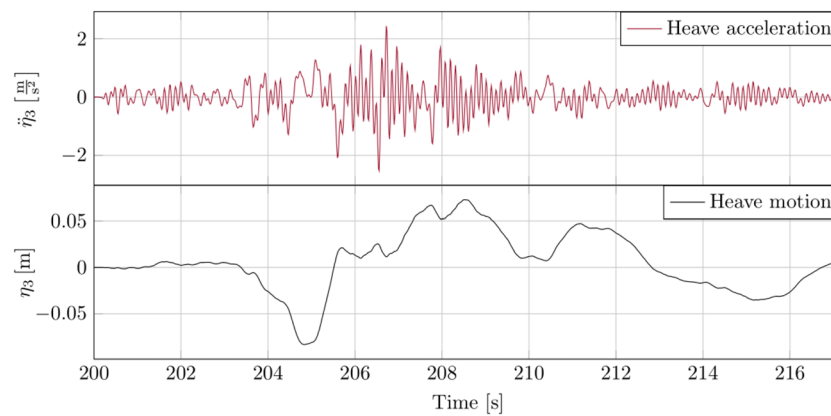


FIGURE 11 Time history of vertical motion of nacelle due to seaquake excitation

TABLE 5 Eigenmodes of the structure in vertical direction

Mode no.	Natural frequency (Hz)	Effective modal mass (%)	Damping ratio
1	9.6	62	0.15
2	25.5	22	0.40
3	47.6	7	0.74
4	70.3	3	1.0

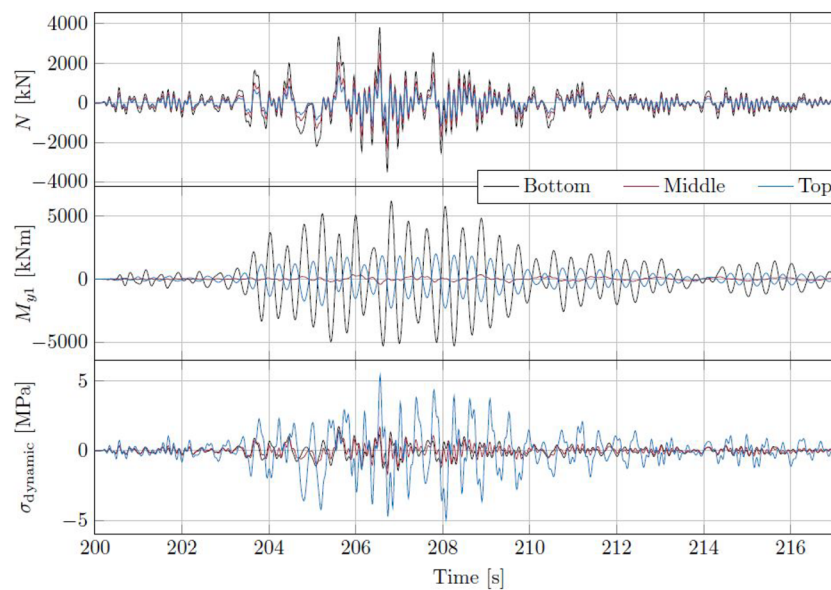


FIGURE 12 Time histories of forces and stresses at different heights in the tower due to seaquake loading.

Of the available response quantities in RIFLEX, the axial force, N , and the bending moment, M_{y1} , are of most interest in the present study. This information is presented and discussed in the following. As described earlier, the seaquake loading was applied to the SIMA model after 200 s of transient response. The static parts of the axial force and the bending moment due to the weight of the RNA and the tower itself were calculated by taking the average value during the interval 100–200 s, and the dynamic axial force and bending moment were obtained by subtracting the corresponding static values. The dynamic part of these response parameters during the seaquake is presented in Figure 12 at the base, middle, and top of the tower (indicated as Elements 1, 14, and 27 in the figure). The maximum dynamic stress occurs at Element 27 (top of tower) with a value approximately 5 MPa. The corresponding static stress is about 22.7 MPa. Comparison of these values indicates that the

seaquake is not critical for the capacity of the tower for the considered level of shaking. Considering the approximately proportional response of the platform to the base acceleration, a strong shaking with $PVA = 0.3$ g would result in a total (static and dynamic) compressive stress of about 70 MPa which is still not governing the design as regards the cross-sectional capacity. However, in an actual design, the buckling capacity should be controlled for these relatively large stresses as the wall thicknesses are small compared with the diameter of the sections. It should be noted that the tower considered here was established for research purposes and is consequently somewhat oversized compared to commercially optimized wind turbine towers.

The other response quantities of interest are the forces in the MLs. Figure 13 shows the configuration of the mooring system and the terms used for the different parts including element numbering in the MLs. The MLs were modeled as RIFLEX bar elements, transferring only the loads from the platform to the anchors as tensile forces. The numbering of the ML elements used in the presentation of the results originates from the discretization in RIFLEX, where each line is divided into two segments. The first segment (S1) comprises the upper 160 m of the lines that was divided into 20 bar elements (elements S1: E1 to E20). The second segment (S2) comprises the remaining 400 m length of the line down to the anchor which was divided into 50 elements (elements S2: E1 to E50).

At the time the seaquake load is applied (at 200 s), the tensile forces in the MLs are approximately 1665 and 970 kN at the top and bottom of the lines, respectively. Figure 14 displays the time histories of the computed tensions in the top and bottom of the mooring elements during the earthquake shaking. Note that the dynamic amplitudes of the forces (i.e., after the initial static offset is subtracted) are about the same in both elements (because no environmental loads are considered in this case, the platform is in a symmetrical position, and the forces in the three lines are practically identical).

Considering the relatively large dynamic oscillations of the tension forces for the considered low shaking, a parametric study was performed by increasing the PVA from 0.05 g to 0.3 g. Figure 15 presents the time histories of the tensions in the ML element connected to the anchor for the selected levels of shaking. It is observed that even a seaquake resulting from a large seabed $PVA = 0.3$ g does not yield a peak mooring tension larger than the estimated extreme value used for design (see next section). However, it is observed that for PVAs larger than 0.15 g the tension falls to zero for a short time interval. The absence of tension in the ML may cause snap tension once the line is loaded again and it needs closer attention in actual design. Even though not studied here, loss of line tension and subsequent snap loads due to seaquakes could be particularly important for TLPs.

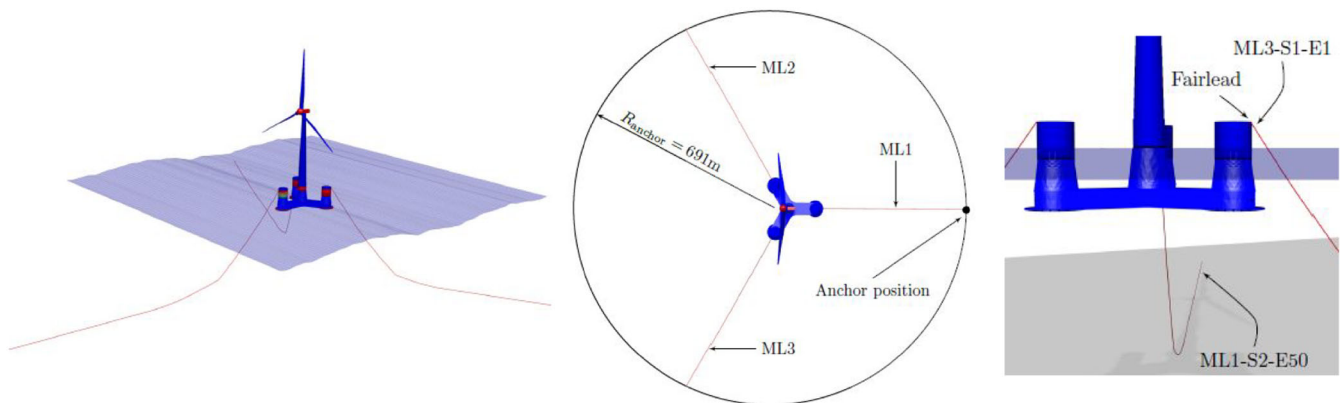


FIGURE 13 Configuration of the mooring system, with nomenclature for different parts, including mooring line (ML) and element numbering.

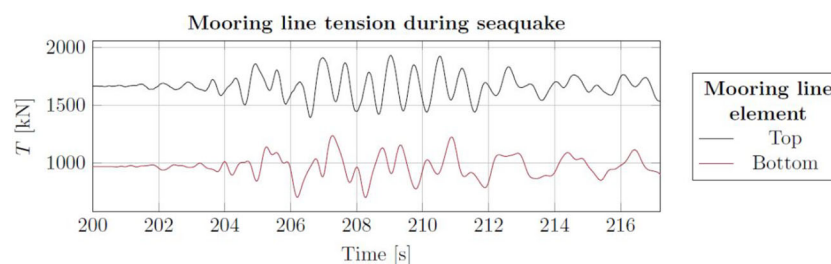


FIGURE 14 Mooring line tensions in top and bottom elements of mooring lines due to platform response during seaquake pressure from 2D acoustic model

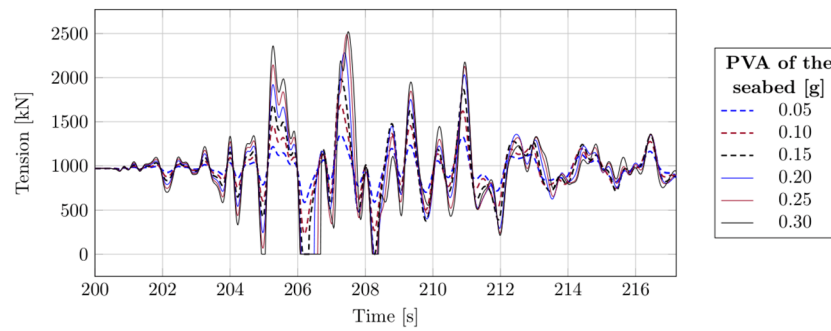


FIGURE 15 Tension in mooring line elements connected to seabed due to earthquakes scaled to different peak vertical accelerations (PVAs)

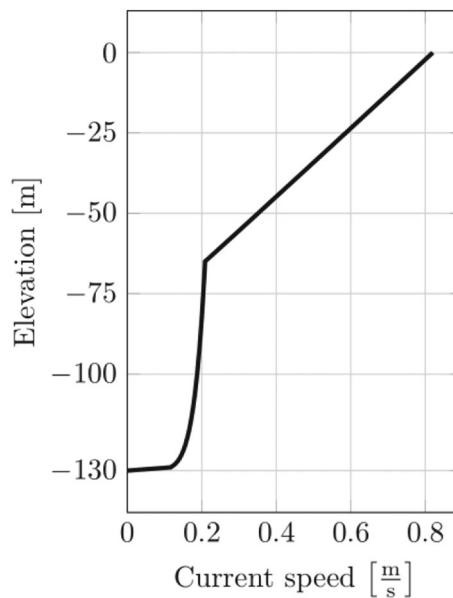


FIGURE 16 Current profile used in simulations

5.2 | Earthquake response during production

In this section, the seaquake response of the FWT during operation is presented. The wind and current were assumed oriented along a direction parallel to the mooring line ML1 with the hub facing the wind. This situation was chosen because it yields a large mean tension in the windward ML and is expected to be the worst situation when the FWT is subjected to the earthquake.

The wind was set to be uniform in the SIMA model with speed corresponding to the rated wind speed of the DTU 10 MW Reference Wind Turbine of 11.4 m/s.²⁶ For practical reasons, no wave load was considered during these analyses as it would complicate the assessment of the effects of the earthquake alone. The current was introduced using the same profile adopted in LIFES50+²⁶ using 1-year reference values of the wind- and tide-induced current speed at the surface equal to 0.59 and 0.23 m/s, respectively. The resulting profile is shown in Figure 16.

For the presentation of the results for the environmental and seaquake loads, the time was initialized after application of the static loads at 200 s, as described in Section 5.1. The initial transient response due to environmental loads was again damped out before application of the seaquake pressures. For the damped model, the platform stabilized at a surge of about 19 m and a pitch of about 4° when subjected to wind and current. The surge motion of the platform tightens the windward ML, while the MLs on the leeward side experience reduced tension. The tensions in the MLs in both the top and bottom elements during the transient response of the damped model, with wind and current applied to the FWT, are displayed in Figure 17. As shown in this figure, the ML element connected to the seabed on the windward side of the FWT (ML1-S2-E50), stabilized at a tension of about 2120 kN compared with 970 kN for the case without any wind or current (Section 5.1). In the opposite end of the ML, in the bar element referred to as ML1-S1-E1, the tension stabilized at approximately 2790 kN compared with 1665 kN without any wind or current.

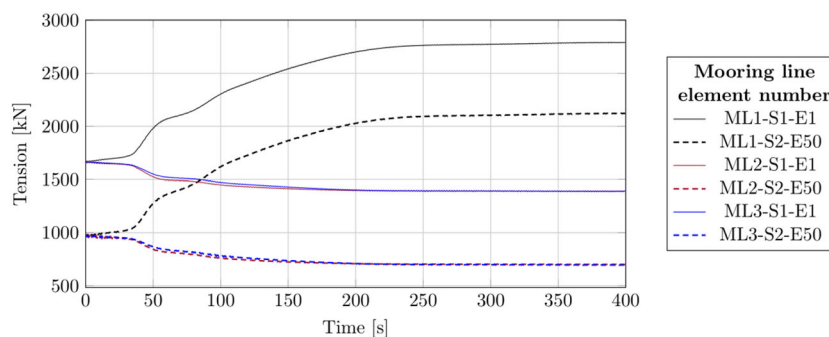


FIGURE 17 Mooring line tension for model with added damping subjected to uniform wind and current (time is initialized after application of static loads at 200 s, ref. to Figure 14)

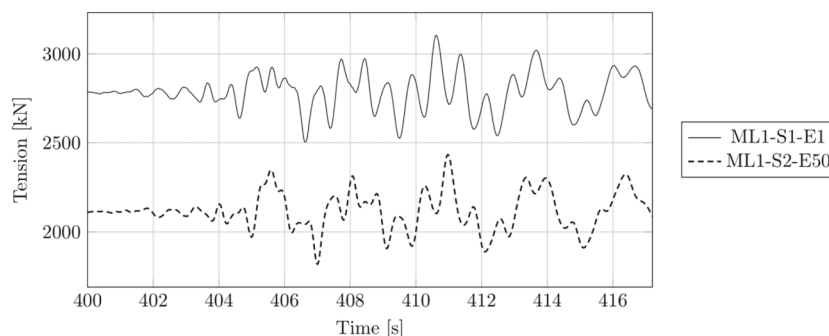


FIGURE 18 Tension at each end of windward mooring line during combined uniform wind, current and seaquake shaking with peak vertical acceleration (PVA) = 0.035 g

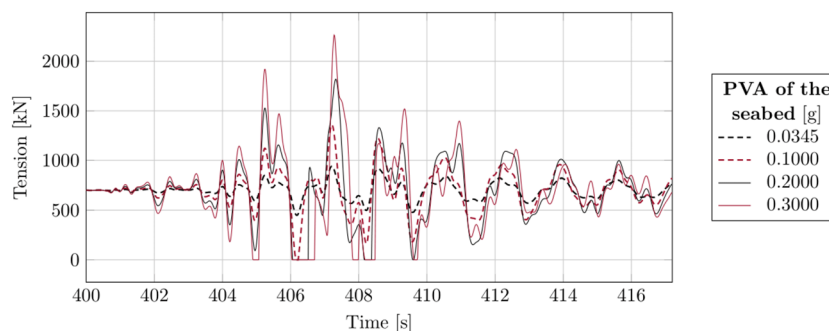


FIGURE 19 Tension in one of the two leeward mooring lines during seaquakes with different peak vertical accelerations (PVAs) together with wind and current loading

The seaquake loading was applied to the model after 400 s of transient damped response. The resulting tension in the windward ML when the FWT is simultaneously subjected to wind, current, and earthquake is presented in Figure 18.

To study the effect of stronger earthquakes on the ML tension, the seaquake pressure was scaled to correspond to different PVAs ranging from 0.1 to 0.3 g. The results indicated that for PVA = 0.1 g, the peak windward ML tension at fairlead and anchor reach about 3100 kN and 2430, respectively, and reach 5020 and 3440 kN for PVA = 0.3 g. The largest peak tension for PVA = 0.3 g is about 64% of the MPM (most probable max) mooring tension calculated based on the extreme value probability distribution of mooring tension at the anchor during environmental loads only.²⁸ A different effect of the combined seaquake, current, and wind loading is the low tensions obtained on the leeward side of the FWT. This is presented in Figure 19 which shows the tensile forces in one of the MLs on the leeward side of the FWT stabilized at approximately 700 kN for the bar element at the bottom of the line, respectively. The figure shows the slack in the leeward lines for PVA values 0.2 and 0.3 g.

6 | PRACTICAL CONSIDERATIONS ABOUT EARTHQUAKE SHAKING

There are several theoretical and practical issues in this subject that warrant discussions. They include accuracy of numerical FE modeling, composition of vertical motions on the ground surface, effect of bedrock's stiffness, and effect of water depth.

1. Accuracy of numerical modeling. This study has confirmed the suitability of the acoustic model in Abaqus for modeling of pressure wave propagation with proper element size and boundary conditions. The problem of wave propagation with the presence of the FWT is 3D by nature. However, it has been shown that one could obtain some indications of the pressure at the base of the FWT from a simple 1D analytical model. For the case considered in this study, a 2D Abaqus model was used to obtain more realistic, but still not accurate, estimates of the pressure for conducting the conceptual modeling in this study. The intention has been to approximately evaluate the impact of vertical earthquake shaking on a typical design. Therefore, one should use and judge the results only on this basis.
2. Composition of vertical ground motions. In the presented analyses, it was assumed that the shaking in the ground (seabed) is due to pressure waves propagating vertically upward in the ground. This is an idealization of the complex earthquake waves and is in line with the common practice of design in earthquake engineering where it is assumed that horizontal ground motions are due only to shear waves propagating vertically in the ground. While this assumption is reasonable for horizontal shaking, its extension to vertical shaking is accompanied by large uncertainties and shortcomings in most cases. A real earthquake is generated at a point at least several kilometers from the ground surface and often at a large distance from the site in consideration. When the earthquake waves impinge on the seabed, a large portion of them propagate along the seabed–water interface as surface Scholte waves within a wavelength in both the ground and the sea. If the earthquake source is deterministically defined, then one could use a seismo-acoustic numerical code such as LAYSAC³⁰ to compute accurately the pressure field at the base of the FWT. The computed pressure can be converted to a force at the base of the platform in the way presented in this study for vertical pressure waves. Unless the earthquake source is approximately below the site, the major component of the vertical seismic motions on the seabed is due to surface waves which do not reach the water surface. Therefore, in most cases, only a small portion of the recorded vertical ground accelerations is indeed due to pressure waves. This has been the reason an earthquake record with a small PVA was selected in this study as it was assumed that the motions are entirely due to vertical pressure waves in the ground. In view of this background, the selected earthquake record could indeed represent a moderate to strong earthquake in most seismic environments.
3. Effect of bedrock's stiffness. The amplitude of pressure waves transmitted to the water is steered by the relationship between the impedances of the bedrock and water. For the 1D analytical solution, the base was assumed rigid (infinite impedance). For this case, the velocity of the water just over the base is the same as that of the base. For the numerical cases considered in Abaqus, it was assumed that the base in the Abaqus model was a bedrock with a pressure wave velocity 5500 m/s resulting in the impedance of the base being about nine times that of the water; therefore, the bedrock practically is like a rigid base. As the impedance of the bedrock is reduced, the particle velocity in the water diminishes. For example, if the impedance of the bedrock is numerically reduced to become equal to that of the water, the particle velocity is halved. For typical stiff soils, the impedance contrast is about 3 which results in certain reduction of the particle velocity in the water.
4. Effect of water depth. As water depth increases, the amplitudes of pressure waves slightly reduce because of damping. However, the most important effect is that the natural frequency of the water column reduces. The natural frequency for the water depth considered in this study is about 3 Hz. This explains the large amplification observed in the response of the wind turbine because this frequency is in the range with dominant earthquake energy. If the water depth is increased to for example 400 m, the natural frequency of the soil column reduces to about 1 Hz for which there is usually remarkably less energy in the vertical earthquake motions. Therefore, the effect of vertical earthquake shaking is expected to be less in deeper waters.

7 | SUMMARY AND CONCLUSIONS

The objective of the present study was to assess the impact of earthquake on response of FWTs. A decoupled approach was adopted in which the seaquake pressures on the base of the FWT from vertical earthquake shaking were computed from a 2D Abaqus acoustic model, and this load was applied to the model of FWT in the hydro-aero-elasto-dynamic code SIMA. It was shown that while an analytical 1D or a 2D model is not able to represent the 3D pressure field generated by an earthquake, they can nevertheless be used to obtain indications of the expected pressures. This is a useful observation especially in large models which pose major computational challenges.

The analyses were performed for a real earthquake record with PVA = 0.035 g on bedrock. Parametric analyses with larger shaking up to 0.3 g were carried out to assess the effect of large earthquakes. The following conclusions were drawn from the analyses.

1. A decoupled analysis provides realistic assessments of seaquake loads for FWT with catenary mooring. For TLP turbines with high vertical natural frequency, one should perform a coupled analysis.

2. Based on the results presented in this study, it appears that even for moderate earthquakes, the seaquake loads combined with normal wind and wave loading are lower than the MPM design loading and can be ignored in design of MLs and anchors. However, it is recommended to assess the structural design of the parts exposed to the seaquake pressure.
3. The pressure waves are amplified in the tower and might result in vertical stresses for large earthquake shaking that could lead to buckling of the steel but probably would not affect the structural capacity of the tower. However, in the present study, a robust tower was considered, and the observation may not hold for commercially optimized towers.
4. The most dramatic effect of earthquake is amplification of the accelerations through the tower all the way to the nacelle. The analyses in this study indicate an amplification of bedrock acceleration by about 7 leading to accelerations typically in the range 0.2 to 0.3 g which are close to the acceptable accelerations during operation. However, these earthquake-induced accelerations happen in very short times and are not expected to have any adverse effects on the design. On the other hand, larger earthquakes with PVAs above 0.2 g will cause accelerations at the nacelle level which may be important to the WTG design.

ACKNOWLEDGMENTS

The authors would like to thank Dr. Petter Andreas Berthelsen at SINTEF Ocean for kindly providing access to SIMA and the OOFs model implemented in SIMA, to Prof. Erin Bachynski-Polić at NTNU for technical discussions and advice on hydrodynamic issues, and to Mr. Matias L. Røvik at Dr. techn. Olav Olsen for sharing his experience on developing the acoustic model in Abaqus. The authors also appreciate the constructive comments by the anonymous reviewers which have improved the quality of the paper.

CONFLICT OF INTEREST

There is no conflict of interest among the authors.

ORCID

Amir M. Kaynia  <https://orcid.org/0000-0002-7774-3860>

REFERENCES

1. Castro-Santos L, Diaz-Casas V. *Floating offshore wind farms*. Springer; 2016. doi:10.1007/978-3-319-27972-5
2. Equinor. How hywind works; 2017a. <https://www.equinor.com/en/what-we-do/oating-wind/howwhywind-works.html>
3. Hove K, Selnes PB, Bungum H. Seaquake: a potential threat to offshore structures. *Symp Behav off-Shore Struct*. 1983;2:561-571.
4. Ambraseys N. A damaging seaquake. *Earthq Eng Struct Dyn*. 1985;13(3):421-424. doi:10.1002/eqe.4290130311
5. Uenishi K, Sakurai S. The generation of seaquakes and its impact on floating bodies. *Int J Protect Struct*. 2014;5(2):207-218. doi:10.1260/2041-4196.5.2.207
6. Matsuoka K. Seismic response of floating structure. *Soc Naval Archit Jpn*. 1988;706:12-18.
7. Kiyokawa T, Inada Y. On the mechanism of seaquakes. *Proc Coast Eng JSCE*. 1989;36:734-738. doi:10.2208/proce1989.36.734
8. Higo Y, Ueno H. A theoretical study on the effect of seaquakes on a floating body. *Trans West-Jpn Soc Naval Archit*. 1997;93:111-119.
9. Baba E. A study on the effect of seaquakes on a floating body. *Proc Jpn Soc Naval Archit Ocean Eng*. 1987;162(162):90-98. doi:10.2534/jjasnaoe1968.1987.162_90
10. Takamura H, Masuda K, Maeda H, Bessho M. A study on the estimation of the seaquake response of a floating structure considering the characteristics of seismic wave propagation in the ground and the water. *J Mar Sci Technol*. 2003;2003(7):164-174.
11. Fujioka K, Nihei Y, Iijima K. Seaquake loads acting on offshore wind turbine. In: *Proc. 35th International Conference on Ocean, Offshore and Arctic Engineering OMAE2016*. Busan, South Korea: BEXCO Exhibition & Convention Center; 2016.
12. Di Pilato M, Perotti F, Fogazzi P. 3D dynamic response of submerged floating tunnels under seismic and hydrodynamic excitation. *Eng Struct*. 2008;30(2008):268-281. doi:10.1016/j.engstruct.2007.04.001
13. Shi C, Domaneschi M, Martinelli L. Nonlinear behaviors of submerged floating tunnels under seismic excitation. *Appl Mech Mater*. 2012;226-228 (2012):1124-1127. doi:10.4028/www.scientific.net/AMM.226-228.1124
14. Martinelli L, Domaneschi M, Shi C. Submerged floating tunnels under seismic motion: vibration mitigation and seaquake effects. *Procedia Eng*. 2016;166(2016):229-246. doi:10.1016/j.proeng.2016.11.546
15. Morison JR, O'Brien MP, Johnson JW, Schaaf SA. The force exerted by surface waves on piles. *Petrol Trans am Inst Mining Eng*. 1950;189(05):149-154. doi:10.2118/950149-G
16. Kaynia AM. Seismic considerations in design of offshore wind turbines. *Soil Dyn Earthq Eng*. 2019;124(2019):399-407. doi:10.1016/j.soildyn.2018.04.038
17. Esfeh PK, Kaynia AM. Numerical modeling of liquefaction and its impact on anchor piles for floating offshore structures. *Soil Dyn Earthq Eng*. 2019;127(2019):105839. doi:10.1016/j.soildyn.2019.105839
18. Chaloulos YK, Tsiapas YZ, Bouckovalas GD. Seismic analysis of a model tension leg supported wind turbine under seabed liquefaction. *Ocean Eng*. 2021;238:109706.
19. Esfeh PK, Kaynia AM. Earthquake response of monopiles and caissons for offshore wind turbines founded in liquefiable soil. *Soil Dyn Earthq Eng*. 2020;136(2020):106213. doi:10.1016/j.soildyn.2020.106213
20. Kjølraug RA, Kaynia AM. Vertical earthquake response of megawatt-sized wind turbine with soil-structure interaction effects. *Earthq Eng Struct Dyn*. 2015;2015(44):2341-2358.
21. Nejad AR, Bachynski EE, Moan T. On tower top axial acceleration and drivetrain responses in a spar-type floating wind turbine. *Proc. ASME 2017 36th International Conference on Ocean, Offshore and Arctic Engineering, OMAE2017-62314*, 2017 doi:10.1115/OMAE2017-62314

22. Dassault Systemes Simulia Corp. *ABAQUS/CAE 6.14-documentation*. Providence, RI, USA: Dassault Systemes Simulia Corp; 2014.
23. Marintek. *Simo - theory manual, version 4.0*. Trondheim, Norway: Marintek; 2012.
24. Dr. techn. Olsen O. Breakthrough for OO-Star Wind Floater; 2020 (<https://www.olavolsen.no/no/aktuelt/post-SdQPQ-gjennombrudd-for-oo-star-wind-oater>)
25. Berthelsen PA. et al. LIFES50+: Innovative floating offshore wind energy. EERA DeepWind'2016, 13th Deep Sea Offshore Wind R&D Conference. Trondheim, Norway; 2016.
26. Bak C et al. Light Rotor: The 10-MW Reference Wind Turbine, Proc. In: *EWEA 2012 - European Wind Energy Conference & Exhibition*. European: Wind Energy Association (EWEA); 2012.
27. Karimirad M. *Offshore energy structures*. Springer International Publishing Switzerland. ISBN 978-3-319-12174-1; 2014. doi:10.1007/978-3-319-12175-8
28. Blekastad H, Schell PAE. *Sequake response of a floating wind turbine*. MSc Thesis,. Trondheim, Norway: Dept. of Structural Engineering, Norwegian University of Science and Technology (NTNU); 2020.
29. Gomez P, Sanchez G, Llana A, Gonzalez G. Qualification of innovative floating substructures for 10 MW wind turbines and water depths greater than 50 m. Report D1.1 Oceanographic and meteorological conditions for the design. H2020 Research Project LIFES50+: Innovative Floating Offshore Wind Energy (<https://lifes50plus.eu/results>); 2015.
30. Park J, Kaynia AM. Stiffness matrices for fluid and anisotropic soil layers with applications in soil dynamics. *Soil Dyn Earthq Eng*. 2018;115(2018):169-182. doi:10.1016/j.soildyn.2018.06.030

How to cite this article: Kaynia AM, Blekastad H, Schell P, Walter EL. Seismic response of floating wind turbines due to seaquakes. *Wind Energy*. 2023;26(2):145-162. doi:10.1002/we.2791